

Short Gamma-Ray Bursts following mergers of a ONeMg with a CO white dwarf

Maxim Lyutikov

Department of Physics, Purdue University, 525 Northwestern Avenue, West Lafayette, IN 47907-2036 and Department of Physics and McGill Space Institute, McGill University, 3600 University Street, Montreal, Quebec H3A 2T8, Canada

and

Silvia Toonen

Astronomical Institute Anton Pannekoek, University of Amsterdam, P.O. Box 94249, 1090 GE, Amsterdam

ABSTRACT

We discuss a scenario of short Gamma-Ray Bursts (GRBs) following a merger of a massive ONeMg white dwarf (WD) with a CO WD, and an ensuing accretion induced collapse (AIC). An initial system with the primary mass $M_1 \sim 6 - 10 M_\odot$ and the secondary mass $M_2 \sim 3 - 6 M_\odot$ forms, via two distinct evolutionary channels, a double degenerate CO-ONeMg WD system. For sufficiently large mass ratio $q \equiv M_2/M_1 > q_{crit} \sim 0.25$ the ensuing gravitational wave-driven mass transfer is unstable, whereby the less massive CO WD is disrupted and transfers its mass to the primary ONeMg WD on a few orbital time scales. The merger product ignites shell CO burning, adding mass to the degenerate core; at the same time mass and angular momentum is lost due to powerful winds. For an ONeMg WD sufficiently close to the Chandrasekhar mass an electron-capture accretion induced collapse (AIC) follows $\sim 10^4$ years afterwards. We associate the prompt short GRB emission with a direct collapse of an ONeMg WD to a neutron star, without formation of an accretion disk. After the collapse the accretion of the unburnt part of the shell onto the newly formed NS powers the extended emission (EE). During the collapse the neutron star is spun to millisecond periods and produce long lasting relativistic winds that shock against the material lost during the shell-burning stage, and produce afterglow emission from the wind termination shock.

1. The problems with NS-NS scenario for short GRBs

The typical duration of Short Gamma-Ray Bursts (GRBs) of ~ 1 second require neutron star-like densities for a dominant energy release, $t \sim 1/\sqrt{G\rho}$. Merger of two neutron stars is

the leading model (*e.g.* Berger 2014). There are problems with the NS-NS paradigm, though, (*e.g.* Lyutikov 2009). The most critical observations that challenge the dominant NS-NS merger paradigm is that a number of short GRBs show powerful extended emission (EE) tails (*e.g.* Norris & Bonnell 2006; Norris et al. 2010) and flares at times as long as 10^5 sec (*e.g.* GRB050724, Gehrels et al. 2009). This runs contrary to many numerical simulations which show that the dominant energy release times scale is tens to hundreds of milliseconds (Hotokezaka et al. 2011; Rezzolla et al. 2010; Sekiguchi et al. 2011; Paschalidis et al. 2015; Ruiz et al. 2016), many orders of magnitude shorter than the duration of the extended tails and occurrence of flares. A small amount of material, $\leq 10^{-2} - 10^{-3}M_{\odot}$, ejected during the merger of unequal-mass neutron stars (*e.g.* Shibata et al. 2017) is accreted on time-scales of 1-10 secs; it is hard to see how this can produce powerful extended emission tails.

The suggestion that a (quasi)-stable neutron star is produced as a result of a neutron star - neutron star merger (Bucciantini et al. 2008; Metzger et al. 2011) requires that the maximal mass of a neutron star is well in excess of $2M_{\odot}$. There is a problem with this assumption. Though the minimal neutron star mass is $1.17M_{\odot}$ (PSR J0453+1559) all the binary neutron star systems have (the well-determined) total mass of $> 2.57M_{\odot}$, see Table 1 (question mark for J1807-2500B indicates that the companion might be a massive WD). During merger some energy will be lost to neutrino, reducing the gravitation mass by $\sim 0.3M_{\odot}$ (*e.g.* Dessart et al. 2009). At the same time development of various shearing instabilities is expected to bring the newly formed neutron star into solid body rotation, eliminating possibility of additional rotational support (*e.g.* Faber & Rasio 2012; Shibata et al. 2017; Baiotti & Rezzolla 2017; Paschalidis & Stergioulas 2016; Paschalidis 2017). Thus, the formation of a stable neutron star as a result of a merger of two neutron stars requires that the equation of state allowed the existence of neutron stars with masses $\geq 2.3M_{\odot}$. But this is the minimum required mass of a stable NS. For the majority of mergers to produce a stable post-merger NS the equation of neutron star matter should allow even higher masses, $\geq 2.5M_{\odot}$.

It is not clear at the moment if centrifugal support or nuclear equations of state may allow formation of neutron stars with masses above $\geq 2.5M_{\odot}$. Below we explore alternative possibilities to produce extended emission. We develop a model that may capture the advantages of producing a millisecond magnetar (Usov 1992) as the central source of short GRBs, yet formed via different channel: electron capture (EC) in the core of a massive ONeMG WD in a binary during the unstable mass transfer.

Table 1: Companion masses and the total mass in binary NSs with well-determined masses. The total mass in all cases is $> 2.57M_{\odot}$. It is highly unlikely that such systems form a stable NS upon merger. Source: [www3.mpi.fr – bonn.mpg.de/staff/pfreire/NS_masses.html](http://www3.mpi.fr/~bonn.mpg.de/staff/pfreire/NS_masses.html).

DNS	M_1	M_2	M_{tot}
J0453+1559	1.559(5)	1.174(4)	2.734(4)
J0737-3039A/B	1.3381(7)	1.2489(7)	2.58708(16)
B1534+12	1.3330(2)	1.3455(2)	2.678463(4)
J17560-2251	1.341(7)	1.230(7)	2.56999(6)
J1807-2500B (?)	1.3655(21)	1.2064(20)	2.57190(73)
J1906+0746	1.291(11)	1.322(11)	2.6134(3)
B1913+16	1.4398(2)	1.3886(2)	2.828378(7)
B2127+11C	1.358(10)	1.354(10)	2.71279(13)

2. WD-WD mergers as short GRB engines

2.1. Previous work: AIC, short GRBs and Type Ia SNe

Most calculations of WD-WD mergers are aimed at explaining the Type Ia SNe, thus *looking* for detonation (see Maoz et al. 2014, for a recent review). Less attention has been given to models that fail to detonate. As we argue below, failed SN Ia, that collapse via electron capture, may be related to the short GRBs. Dan et al. (2014) discussed the results of the WD-WD mergers and argued that there is large phase space available for WD-WD mergers to produce an accretion induced collapse (AIC). Nomoto & Iben (1985) stressed the role of carbon ignition during WD mergers in order to produce a Type Ia SN. Thus, in order to avoid explosion, there should be little carbon in the system.

The electron capture mechanism, the key physical process behind the AIC, was suggested by Canal & Schatzman (1976). The most often discussed observational evidence of AIC of WD is the alternative possibility of forming MSPs (*e.g.* Bhattacharya & van den Heuvel 1991; Hurley et al. 2010). Tauris et al. (2013) discussed a similar scenario that may lead to the formation of MSPs, including a list of systems that might have formed via AIC.

Previously, several papers discussed a possibility, with a few variations, of AIC as the central engine of short GRBs (Duncan & Thompson 1992; Vietri & Stella 1999; Dessart et al. 2007; Metzger et al. 2009b; King et al. 2001; Levan et al. 2006; Lee & Ramirez-Ruiz 2007; Piro & Kulkarni 2013). The dominant theme is the formation of a highly magnetized rapidly spinning neutron star, that loses its rotational energy by a highly magnetized wind. For example, Metzger et al. (2009a) discussed the case of fast initial rotation that results in a formation of a disk. Piro & Kulkarni (2013) discussed the possible radio signal from the

AIC of a WD.

We stress somewhat different aspects of the AIC. First, we discuss in more details the evolutionary scenarios that lead to AIC, highlighting the importance of one companion being a heavy ONeMg WD (to avoid detonation during unstable mass transfer), the formation of a shell-burning star, post-AIC shell accretion and post-accretion spin-down.

Regarding the origin of Type Ia SNe, our model is both somewhat independent of the active discussions on single versus double degenerate/mixed origin of SNIa (in a sense that it can work in both cases), but at the same time the model is closely related to the controversy. As a working assumption, we assume the double degenerate super-Chandrasekhar CO-CO WDs scenario for SNIa. The merger of ONeMg-CO WDs will likely proceed in a very different regime.

2.2. Rates of WD mergers and short GRBs

The synthetic rate of CO+CO WD mergers with a combined mass exceeding the Chandrasekhar limit (see e.g. Claeys et al. 2014; Wang & Han 2012, for overviews) approaches the most recent observational estimates of the SNIa rate (Maoz & Graur 2017) by a factor of a few. The Galactic SNIa rate (several 10^{-3} yr $^{-1}$ Cappellaro & Turatto 2001) is much higher than the rate of short GRBs (several 10^{-6} yr $^{-1}$ Berger 2014; Coward et al. 2012). Thus, it is required that only a few percent of WD-WD mergers exceeding the Chandrasekhar mass produce a short GRB. Other works (*e.g.* Lee & Ramirez-Ruiz 2007) came to similar conclusion: only about 1% of WD-WD mergers are needed to account for the short GRB rate. Our population synthesis calculations generally correspond to these findings as well, see Sect. 3.

Thus, importantly, we are looking for a narrow parameter range in the pre-merger WDs masses and compositions, and possibly spins (and correspondingly narrow parameter range in the main sequence masses and separations) that may lead to the production of the short GRBs from the double white dwarfs (DWDs) mergers. Most DWD mergers do not lead to short GRBs.

2.3. Spatial Distribution

Short GRBs approximately track stellar mass, not light like the long GRBs (Berger 2014). They also have wide distribution of off-set distances from the centers of the host galaxies (Berger 2010). Berger (2014) noted a similarity between the distribution of short

GRBs and Type Ia SN progenitors. In the present model this is natural consequence as the two phenomena come from nearly the same progenitors (assuming a double degenerate model for Type Ia SNe).

One of the possible problems for the present model is a wide distribution of the offset distances from the centers of the host galaxies for short GRBs (Berger 2010). It is not clear whether the NS-NS binaries fare much better, though (Voss & Tauris 2003, studied distribution of merging neutron stars). Typical velocities of NS binaries is tens of kilometers per second (Tauris, priv. comm.; only PSR B1913+16 has 240 km s^{-1}). Presumably, higher kicks disrupt a binary. These velocities are not too different from the velocity dispersion in the Galaxy, only slightly higher. WD-WD binaries are expected to have smaller velocity, but this will be partially compensated by more extended location of the origin of the WD binaries (many in halos and globular clusters) compared to the NS binaries (which originate from the galactic disk.) We acknowledge a possible issue with the distribution of merging WD binaries with respect to the host galaxy as sources of GRBs.

2.4. Hints from collapse physics

The merger of WDs is a leading model to explain SN Ia (van Kerkwijk et al. 2010; Pakmor et al. 2010; Shen et al. 2017). To explain short GRBs detonation should be avoided - in the present model the accretor is a heavy ONeMg WDs, not a more common CO WD. Also, the donor is a degenerate star, *e.g.* run of the mill CO WD with $M \sim 0.65M_{\odot}$ (so that the final mass transfer proceeds in unstable regime). The reason is that ONeMg WD accreting from another WD is more likely to collapse than explode (see, *e.g.* Schwab et al. 2015) due to

- Both H-burning and He-burning are usually unstable (*e.g.* Townsley & Bildsten 2005), resulting in the ejection of the most of the accreted mass. Thus, to bring a WD over the Chandrasekhar limit the donor must be an evolved star with no hydrogen or helium.
- Most white dwarfs of moderate mass have a C/O composition. Carbon and oxygen are very prone to fusion reactions. The neutronisation thresholds for O, Ne, Mg are all lower than for C, implying that (i) they are more susceptible to collapse; (ii) are less likely to trigger C burning/SN Ia explosion.

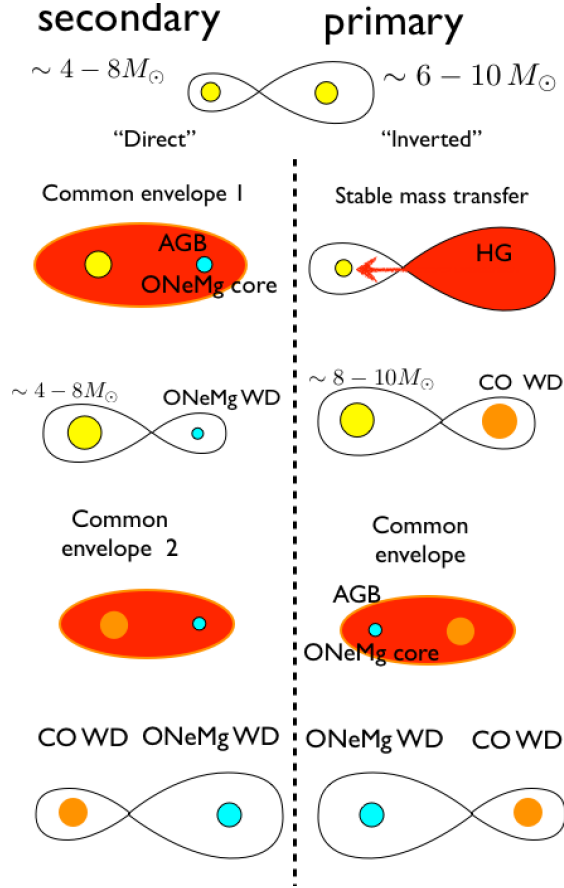


Fig. 1.— Pre-merger evolutionary scenarios: direct channel (left column) and inverted channel (right column).

2.5. Evolutionary scenario: pre-merger evolutionary tracks

In Fig. 1 we picture the evolutionary scenario leading to the short GRB. There are two evolutionary paths that can lead to the formation of a ONeMg-CO WD binary, that we call direct and inverted. In the direct scenario, applicable to large initial separations, the ONeMg WD is formed first, while in the inverted scenario, applicable to smaller initial separations, the primary transfers a lot of mass onto the secondary, so that the ONeMg WD is formed second. Let us discuss these scenarios in turn.

2.5.1. *Direct formation of ONeMg-CO WD binary, Fig. 1 left column.*

- **First Common Envelope phase and formation of a ONeMg WD.** The binary starts with two unequal mass main sequence stars, Fig. 3, with the primary near the upper limit for ONeMg WD formation, $M_1 \approx 7 - 10M_\odot$ (Langer 2012). (The primary should avoid EC SNe, see Podsiadlowski et al. 2004). Initial separation is large high, on the order of hundreds/thousands of Solar radii, Fig. 4. As the primary starts evolving, its radius increases, up to few $10^3 R_\odot$ - for smaller separations the system will enter the First Common Envelope stage, CE-I (Ivanova et al. 2013). For sufficiently large initial separation the primary will enter the CE-I at the (super-)AGB stage (Siess 2006), so its core is already a ONeMg WD. During the CE-I the orbital separation decreases, while the mass of the primary reduces to $\sim 1.3M_\odot$ both due to wind and loss of envelope during the CE-I. The mass of the secondary does not increase much (Ivanova et al. 2013).
- **Second Common Envelope phase.** The primary is an ONeMg WD with $\sim 1.3M_\odot$, secondary is a Main Sequence star with $3 - 5M_\odot$. The companion starts evolving, enters the giant branch and fills its Roche lobe. Mass loss via Roche lobe overflow results in expansion of the star, dynamically unstable mass transfer and the formation of a second common envelope stage, CE-II (Paczynski 1971; Iben & Livio 1993; Ivanova et al. 2013). The system can survive the CE-II phase (Ivanova et al. 2013). After this stage, the system is going to consist of a ONeMg primary and CO secondary WDs.

We note that massive stars can instigate more than one phase of mass transfer. Once mass transfer as discussed above ceases, the old donor star evolves further. Helium burning takes place in its core or in a shell surrounding the core, which in its turn is surrounded by an envelope of hydrogen-poor helium-rich material. As this star evolves further, it can fill its Roche lobe again, leading to Case BB RLO (Tauris et al. 2012). This additional post-mass-transfer phase is a result of the naked helium star (the stripped core of the original donor star) filling its Roche lobe when it expands to become a giant during helium shell burning. For simplicity we do not include it in Fig. 1. It is included in the simulations described in Sect. 3.

2.5.2. *Inverted formation of ONeMg-CO WD binary, Fig. 1 left column.*

- **Stable mass transfer.** At smaller initial smaller separations, the mass transfer can take a form of Roche Lobe overflow, at the Hertzsprung-gap stage of the primary, with a large amount of mass transferred to the secondary (Toonen et al. 2012; Mennekens

et al. 2010). As a result, the primary forms a CO WD, while the secondary’s mass reaches $\geq 7M_{\odot}$.

- **Common Envelope phase.** The primary is a CO WD with $\sim 0.9M_{\odot}$, secondary is a Main Sequence star with $7-10M_{\odot}$. The companion starts evolving, enters the red giant branch, fills its Roche lobe; dynamically unstable mass transfer leads to the formation of a second common envelope stage. Eventually, the secondary forms a ONeMg WD. After this stage, the system consists of a ONeMg secondary and CO WDs primary.

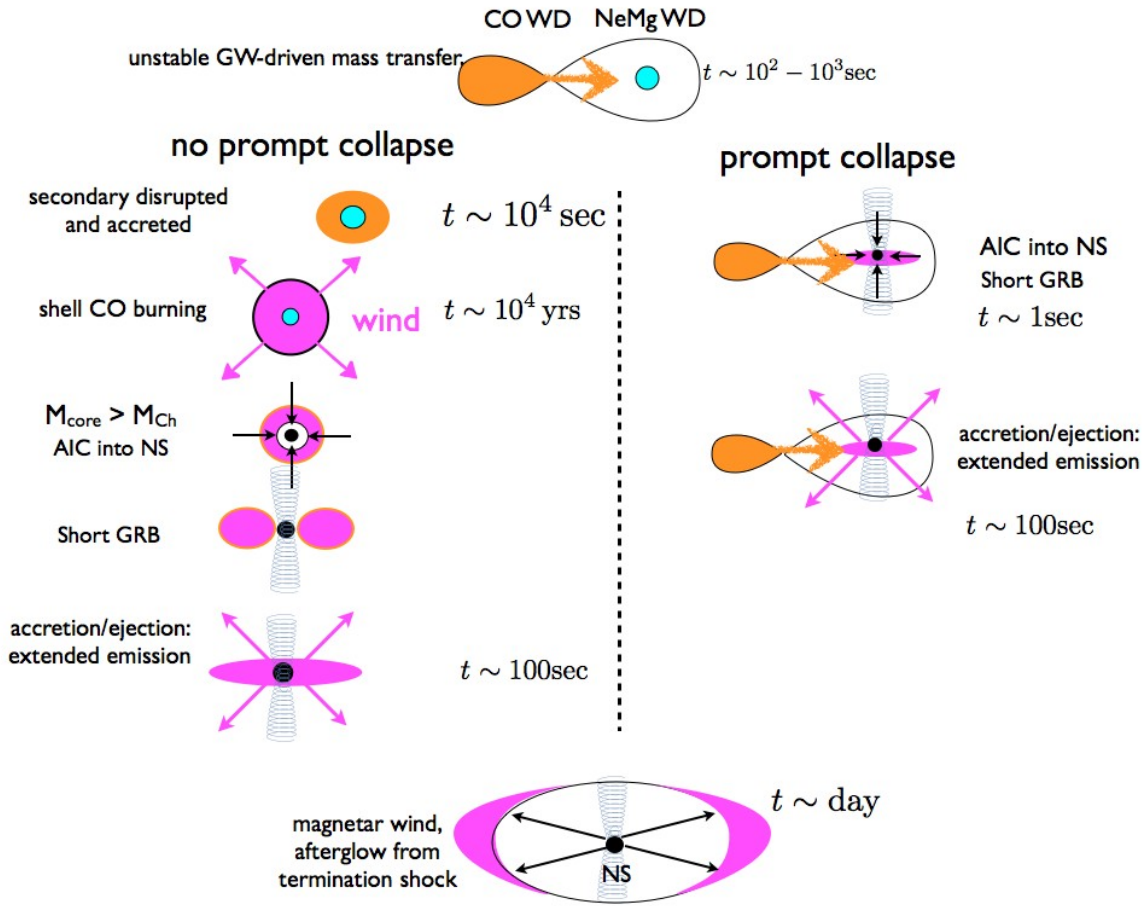


Fig. 2.— Post-merger evolutionary scenarios. As our basic scenario we chose left column - no prompt collapse, CO shell burning and AIC after the core exceeds M_{Ch} .

2.6. WD-WD mergers

Let us next discuss, somewhat independently from the previous discussion of evolutionary scenarios, how mergers of ONeMg and CO WDs may lead to the production of short GRBs. (The case of less massive WD being a He WD is also possible, but disfavor this case since (i) accretion of He is likely to proceed explosively (Pakmor et al. 2013); (ii) smaller mass ratios are more likely to produce stable mass transfer - see, though Shen et al. (2012).) In the scenario we describe below many steps are controversial, and not all are calculated in detail in this work, or generally agreed upon. Yet the the following discussion is a reasonable description of what may happen.

2.6.1. ONeMg-CO WD merger with shell burning, Fig. 2, left column

- **Gravitational-wave driven unstable mass transfer.** For sufficiently close WD binary, emission of gravitational waves leads to the orbital shrinking; the CO WD starts to fill its Roche lobe, and starts transferring mass onto the primary. As long as the mass ratio is above critical $q > q_c \approx 0.25$, the mass transfer is unstable - as matter flows from the less massive CO WD onto the more massive ONeMg WD, the orbit expands. For example, Marsh et al. (2004) discuss different regimes of mass transfer in DD systems, they find that for $M_\odot \sim 1.1 - 1.3M_\odot$ the mass transfer can be unstable for $q \geq 0.25$ (see also simulations by Staff et al. (2012) and discussion by Motl et al. (2017)). At the same time, the CO WD expands as well (less massive WDs have larger radii). In case of unstable mass transfer the expansion of the WD over-compensates for the orbital expansion. As a result, the companion is disrupted on few orbital time scales (*e.g.* D’Souza et al. 2006).

Most interacting double WD binaries are likely to merge, as oppose to experience dynamically stable mass transfer (Shen 2015). We assume that the mass transferred onto the primary ONeMg WD is not detonated in SN Ia event (ONeMg is hard to ignite; *e.g.* Raskin et al. 2012), nor that the shell is ignited in nova-like outburst.¹ Thus, during the unstable mass transfer the companion is fully disrupted and accreted onto the collapsed primary (Webbink & Iben 1987; Iben 1988).

- **Shell burning above ONeMg core.** After the disrupted CO WD is accreted, the shell is viscously spread-out over the core on a timescale of $\sim 10^4$ seconds Yoon et al.

¹Note that even if mass transfer between a He WD and a ONe WD is unstable, the contribution to the merger rate is a few percent at best, as only few He-ONe DWDs are formed.

(2007); Shen et al. (2012). Stable nuclear burning is ignited at the base of the shell, adding mass to the degenerate core. The ONeMg core is not ignited. At the same time powerful winds lead to mass loss and angular momentum loss from the envelope. The overall luminosity is of the order of Eddington luminosity. At this stage there a competition between the wind mass loss from the shell, and the addition of degenerate material to the core. Under certain condition the wind mass loss dominates, and the core never reaches M_{Ch} . (Magnetic White Dwarf EUVE J0317-85.5 with $M = 1.35M_{\odot}$ could be an example of such "near the cliff" WD that nearly underwent AIC - if few hundredths of M_{\odot} would have been added.

- **AIC.** After the total mass of the core exceeds the Chandrasekhar limit, AIC of a WD to NS follows (Saio & Nomoto 1985; Kawai et al. 1987; Mochkovitch & Livio 1990; Miyaji et al. 1980; King et al. 2001; Schwab et al. 2016). The AIC proceeds inside-out - the core bounce is the first observed effect. Core-bounce leads to an outgoing shock that may create a weak supernova-like explosion (Woosley & Baron 1992; Dessart et al. 2006; Kitaura et al. 2006; Abdikamalov et al. 2010; Nakar & Sari 2012; Fryer et al. 1999). The outgoing material also has to plow through the still remaining shell, remains of the disrupted companion. This material will modify the observed properties of the explosion.
- **Magnetic fields and jets - the short GRB.** The primary ONeMg WD is slowly rotating before the onset of the unstable mass transfer. It is spun up during the unstable mass transfer, but a lot of angular momentum is lost (Shen et al. 2012). For sufficiently slow rotation before the AIC, the collapse is direct, without formation of the accretion disk. In this case the collapse of the core proceeds on dynamic, not viscous time scale. During the core collapse differential rotation amplifies B-field (Thompson & Duncan 1995) and produces an MHD jet (Burrows et al. 2007, give estimates of magnetic field amplification during collapse). On the other hand, the shell, the disrupted CO companion with $M \sim 0.1 - 0.5M_{\odot}$ remaining after shell burning and wind loss, forms a disk that helps confine mildly collimated outflow. Since there is little envelope to collimate the outflow (only a fraction of the Solar mass, not few solar masses as in the case of core-collapse SNe), the jet is wide and terminates quickly. These are the Short GRBs. Importantly, the expected duration is not a free-fall time for WD to collapse, but the bounce time, corresponding to the size of the proto-neutron star.
- **Continuing accretion - the extended emission.** The disk formed from the shell accretes on time scale $\sim 100 - 1000$ seconds, but the primary is now a neutron star. Thus, the newly formed neutron star experiences mild accretion rates on the viscous time scale of a few orbital periods. This powers the EE.

- **Wind from isolated NS - early afterglow.** AIC may spin-up the resulting neutron star to millisecond periods and amplify magnetic field to magnetar values, creating conditions favorable for magnetar-driven out flows (*e.g.* Metzger et al. 2008). After the disk is accreted/ejected, the nature of the collimation changes - isolated neutron stars form equatorially, not axially collimated outflows, with power $\propto \sin^2 \theta$ (Michel 1973, θ is the polar angle). (This important point was not stressed by previous models invoking millisecond magnetar as a central source of short GRBs. Conventionally, models of prompt emission, both in long and short GRBs, rely on axially collimated jets (*e.g.* MacFadyen & Woosley 1999; Rezzolla et al. 2011). Intrinsically, rotating neutron stars produce more power in the equatorial direction. If a heavy medium is present, *e.g.* outer layers of a collapsing star, the outflow can be collimated (Metzger et al. 2011; Komissarov et al. 2009) in a way similar to the outflows in the Crab Nebula (Komissarov & Lyubarsky 2003, 2004).)

As the highly relativistic wind from the newly formed NS interacts with the expelled shell, and with the pre-collapse wind, a termination shock is formed. The shock is relativistic and highly magnetized. The wind termination shock produces afterglows in a manner similar to the case of long GRBs, as discussed by Lyutikov & Camilo Jaramillo (2017).

2.6.2. *ONeMg-CO WD merger with prompt AIC, Fig. 2, right column*

A somewhat alternative possibility is that the ONeMg is very close to the Chandrasekhar limit at the beginning of the unstable mass transfer. As the accreted material is heated, it loses degeneracy and thus exerts little pressure on the ONeMg core. Still, if the mass of the ONeMg WD is sufficiently close to the Chandrasekhar limit this extra force may be sufficient to induce AIC before the disruption of the CO WD is completed. The ensuing evolution will resemble NS-WD disruption events (*e.g.* Bobrick et al. 2017).

3. Population synthesis

Using the binary population synthesis (BPS) code `SeBa` (Portegies Zwart & Verbunt 1996; Toonen et al. 2012; Toonen & Nelemans 2013), we simulate the evolution of a large number of binaries following in detail those that lead to the merger of an ONeMg and CO WD. Processes such as wind mass loss, stable & unstable mass transfer, accretion, angular momentum loss, and gravitational wave emission are taken into account. It was shown by Toonen et al. (2014) that the main source of uncertainty in the BPS outcomes come from the

uncertainty in the input assumptions, in particular the CE-phase. For this reason, we follow Toonen et al. (2012), in performing two sets of population synthesis calculations using their model $\alpha\alpha$ and $\gamma\alpha$. For full details on the models, see Toonen et al. (2012). In short, these models differ from one another with respect to the modeling of the CE-phase. Despite the importance of this phase for the formation of compact binaries and the enormous effort of the community, the CE-phase is still poorly constrained (see Ivanova et al. 2013, for a review). Commonly the CE-phase is modeled in BPS codes by energy conservation (Webbink 1984), with a parameter α that describes the efficiency with which orbital energy is consumed to unbind the CE. This recipe is used in model $\alpha\alpha$ for every CE-phase. An alternative model has been proposed by (Nelemans et al. 2000) in order to reproduce the observed population of double white dwarfs. This model is based on a balance of angular momentum with an efficiency parameter γ . In our model $\gamma\alpha$, the γ -recipe is used unless the binary contains a compact object or the CE is triggered by a tidal instability (rather than dynamically unstable Roche lobe overflow, as proposed by Nelemans et al. (2000) for detached double white dwarfs.

Figures 3-4 show the initial parameters of binaries leading to mergers between ONeMg and CO WDs in our simulations. Every point represents a single system in the BPS simulations. The figures show that there are different evolutionary paths that can lead to an ONe-CO WD merger, however the dominant channels involve initially compact systems (in blue circles) i.e. the 'inverted channel' and initially wide systems (in green squares) i.e the 'direct' channel. For single stars, the initial mass of the progenitor of an ONeMg WD ranges between approximately $6.5-8M_{\odot}$ according to SeBa. This is similar to the range of initial masses in the direct channel where the primary forms the ONeMg WD (majority of green points in Fig. 3). The progenitors of ONeMg WDs in the 'inverted' channel, *i.e.* the secondaries denoted in blue, have lower masses as these stars accrete a significant amount of mass from their companion stars.

In Fig. 5 we show the final masses of the ONeMg and CO WD that merge according to model $\alpha\alpha$ and $\gamma\alpha$ respectively. The masses of the ONeMg WDs are in the range $1.1-1.4M_{\odot}$, while the majority of CO WDs have masses in the range $0.5-0.8M_{\odot}$. As described in Sect. 2.5, it is possible that the ONeMg WD forms before the other WD in the system (channel 'direct'), or it forms afterwards (channel 'inverted'). In model $\gamma\alpha$, 48% of merging ONe-CO DWDs go through the 'direct' channel, whereas for model $\alpha\alpha$ the fraction goes up to 69%. The masses of the CO WDs in the 'inverted' channel are systematically higher than those of the 'direct' channel.

In Fig. 6 we show the distribution of the mass ratio as a function of the primary mass. For donor masses in the range $1.1-1.3M_{\odot}$ Marsh et al. (2004) (see their Fig. 1) find that

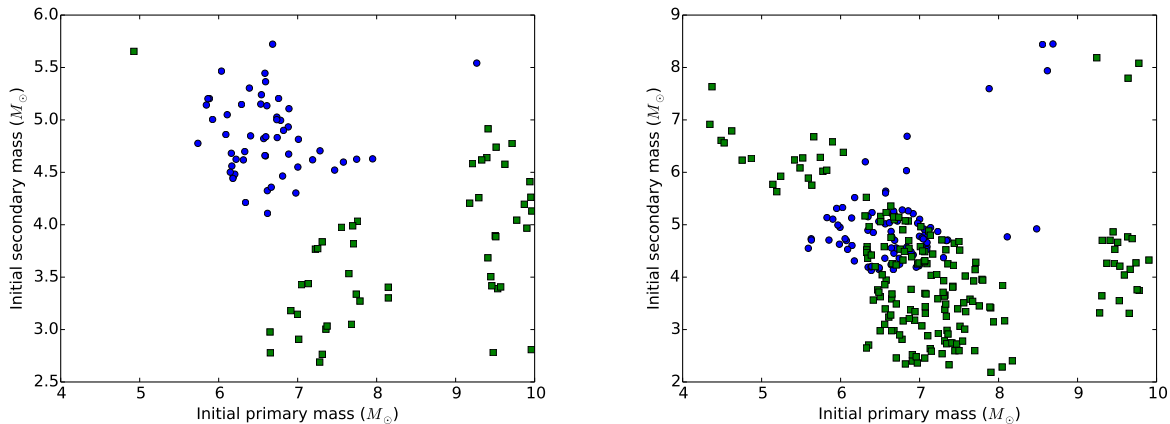


Fig. 3.— Distribution of initial masses for model $\gamma\alpha$ (left panel) and model $\alpha\alpha$ (right panel). The primary represents the first formed WD, secondary the last formed WD. With green squares the systems where the ONeMg WD is formed first, with blue circles where this is the last formed WD. In all models the systems marked in blue come from tight orbits where the first phase of mass transfer is likely stable mass transfer. The systems marked in green mostly originate from wider orbits, such that that first phase of mass transfer is likely a common-envelope phase.

mass transfer is always unstable if the companion mass is above ~ 0.6 . It is always stable for $\leq 0.2 - 0.4$. The blue systems are well above the limit for unstable mass transfer. The green systems occupy a larger part of parameter space. The far majority of the systems have a mass ratio that make stable mass transfer unlikely. Also note that given the 'optimistic' stability limits of Marsh et al. (2004) the AM CVn rate is overestimated by orders of magnitude, indicating that mass transfer is likely less stable than the 'optimistic scenario'. In addition, the results from Marsh et al. (2004) do not take into account the effect of novae outbursts on the evolution of the systems. As shown by Shen et al. (2012) these outburst have a destabilizing effect on the mass transfer.

Assuming a constant Galactic star formation rate of $6M_{\odot} \text{ yr}^{-1}$ for the last 10 Gyr², the current merger rate of CO-ONeMg WDs is $1.9 \times 10^{-4} \text{ yr}^{-1}$ for model $\gamma\alpha$ and $5.0 \times 10^{-4} \text{ yr}^{-1}$ for model $\alpha\alpha$. This is still approximately an order of magnitude higher than the estimated short GRB rate. Thus, even among the ONeMg-CO WD mergers, only about $\sim 10\%$ need to produce a short GRB. (This conclusion strongly depends on the assumed beaming of short

²The assumed star formation history is normalized, such that the total stellar mass corresponds to the Galactic stellar mass of $6 \times 10^{10} M_{\odot} \text{ yr}^{-1}$ (Toonen et al. 2017)

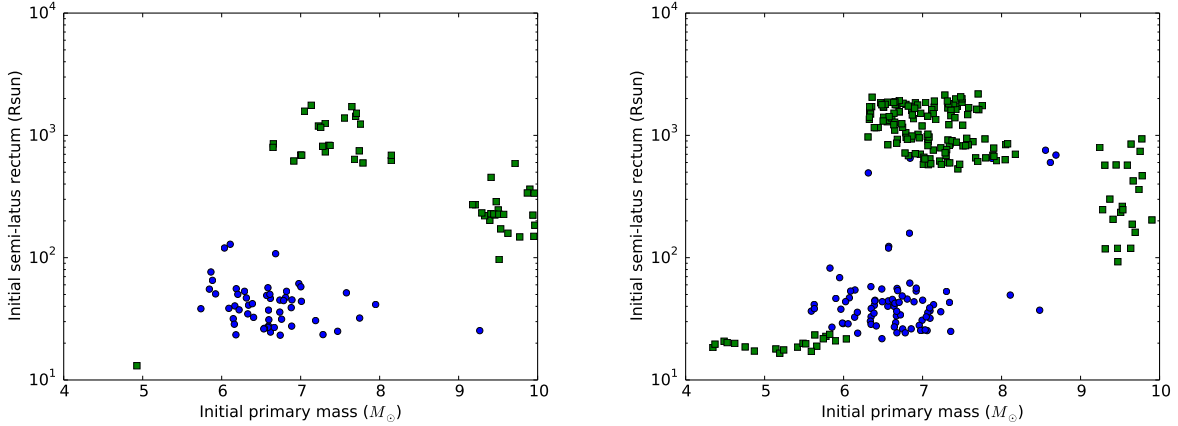


Fig. 4.— Distribution of initial semi-latus rectum for model $\gamma\alpha$ (left panel) and model $\alpha\alpha$ (right panel). The color coding is the same as in Fig. 3. In the case of $\alpha\alpha$, green dots at low orbital separations correspond to the systems in which the primary starts with $\sim 6M_\odot$ and relatively small separation, so that the first phase of mass transfer is stable. As the secondary accretes, it becomes more massive, its evolution speeds up, and it becomes a ONeMg WD while the primary is still a stripped (hydrogen poor helium-rich) nuclear burning star, which eventually becomes a WD. This is similar to the third evolution channel in Toonen et al. (2012).

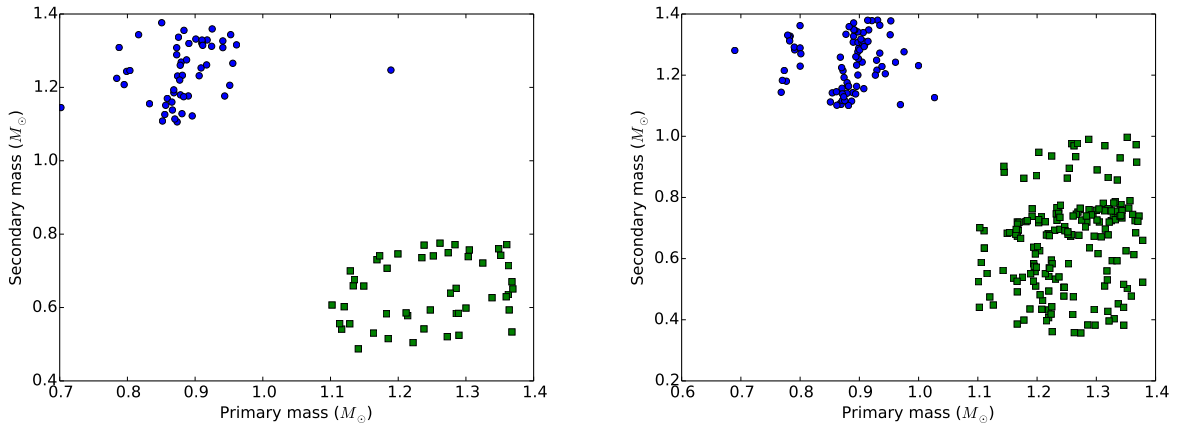


Fig. 5.— Distribution of masses for model $\gamma\alpha$ (left panel) and model $\alpha\alpha$ (right panel). The color coding is the same as in Fig. 3.

GRBs.)

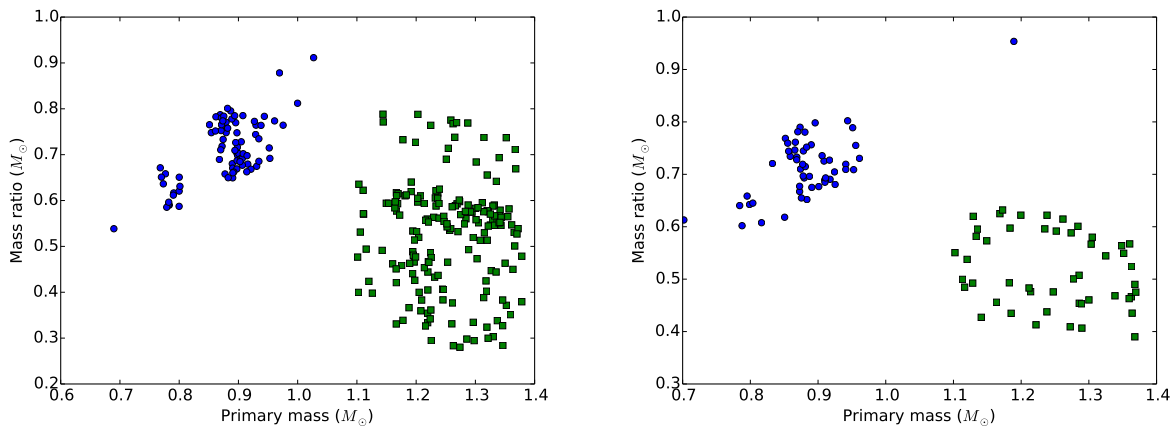


Fig. 6.— Distribution of the mass ratio as a function of the primary mass for model $\gamma\alpha$ (left panel) and model $\alpha\alpha$ (right panel). The color coding is the same as in Fig. 3.

4. Unstable mass transfer in WD-WD binary

4.1. Stellar and orbital parameters

Consider a WD binary with primary mass $M_1 = 1.3M_\odot$ and companion $M_2 = 0.65M_\odot$ (so, $q = 1/2$) and assume that the critical value for unstable mass transfer is $q_{crit} \leq q$. As long as $q_{crit} \leq q$ exact value of q_{crit} is not important (q_{crit} can be as small as 0.25, *e.g.* Benz et al. 1990; D’Souza et al. 2006; Motl et al. 2007); also, the unstable mass transfer is typically not stabilized (Shen et al. 2012). The secondary enters the Roche lobe when the size of the WD R_{WD} becomes of the order of the Roche lobe R_{RI} .

$$R_{WD} = \frac{(9\pi)^{2/3}}{8} \frac{\hbar^2}{Gm_e M_2^{1/3} m_p^{5/3}} \quad (1)$$

$$R_{RI} = 0.46224a_0 \left(\frac{q}{1+q} \right)^{1/3} \quad (2)$$

(where for qualitative estimates we use a simple expression for the WD radius R_{WD} and the size of the Roche lobe R_{RI} ; for more precise values see (Eggleton 1983), and assume a simple ideal non-relativistic EoS for the companion WD). For a $M_1 = 1.3M_\odot$ primary and $q = M_2/M_1 = 1/2$ this occurs when the orbital separation a_0 is

$$a_0 = \frac{1.7(1+q)^{1/3}\hbar^2}{GM_1^{1/3}q^{2/3}m_em_p^{5/3}} = 1.2 \times 10^9 \text{ cm} \quad (3)$$

The gravitational wave-driven inspiral timescale at that moment,

$$\tau_G = \frac{5a_0^4 c^5}{32G^3 M_1 M_2 (M_1 + M_2)} = 2.0 \times 10^9 \text{sec}, \quad (4)$$

is much longer than the orbital period

$$P_{orb} = \frac{2\pi a_0^{3/2}}{\sqrt{G(M_1 + M_2)}} = 16 \text{sec} \quad (5)$$

The estimates above use highly idealized equation of state and a simple prescription for the size of the Roche lobes; they should be taken only as order-of-magnitude estimates.

4.2. Spin evolution of the merger product

During unstable mass transfer the lighter WD is disrupted and forms a disk around the primary. Disk accretion at high rates creates a spreading layer - a belt-like structure on the surface of the primary Inogamov & Sunyaev (1999); Balsara et al. (2009); Inogamov & Sunyaev (2010); Belyaev et al. (2013); Philippov et al. (2016). After the spreading is complete (on viscous time scale of $\sim 10^4$ seconds, *e.g.* Shen et al. 2012) the resulting star of $\sim 2M_\odot$ consists of a slowly rotating degenerate ONeMg core, and a fast rotating, with period in the hundreds of seconds, non-degenerate envelope. After the removal of the degeneracy the envelope expands to $R_{shell} \sim \text{few } 10^9$ cm. The star will emit near Eddington limit and drive powerful winds. Angular momentum contained in the shell will be both lost to the wind, and transported to the core through the (turbulent) boundary layer.

The moment of inertial of the merger product is a sum of the moment of inertia of the core $\eta_0 M_1 R_1^2$ (η_0 is the gyro-ratio - the moment of inertia divided by MR^2) and of the envelope, $\approx M_2 R_{shell}^2$. The contribution from the envelope - the disrupted companion - dominates:

$$\frac{\eta M_1 R_1^2}{M_2 R_{shell}^2} \approx 10^{-3} \quad (6)$$

for $R_1 = 3000$ km and $q = 1/2$. Thus, we expect that the core quickly comes into solid body rotation with the envelop.

To estimate the angular velocity of the shell we note that after accretion the shell quickly expands to R_{shell} ; this expansion decreases its angular velocity. As an estimate of the shell's spin we can equate the proper angular momentum of the companion, $\sqrt{a}\sqrt{GM_1}^{3/2} q/\sqrt{1+q}$, at the point of merger (3) to the angular momentum of the shell, $R_{shell}^2 \Omega_{shell}$. We find

$$\Omega_{shell} = \frac{3^{5/6} \pi^{1/3}}{2^{7/6} \sqrt{5}} \frac{M_1^{1/3} \hbar}{q^{1/6} \sqrt{q+1} R_{shell}^2 \sqrt{m_e m_p}^{5/6}} = 8 \times 10^{-3} \left(\frac{R_{shell}}{5 \times 10^9 \text{cm}} \right)^{-2} \text{s}^{-1}, \quad (7)$$

so that the shell rotates with a period of about 700 seconds. This estimate agrees with more detailed calculations (Benz et al. 1990; Raskin et al. 2012; Shen et al. 2012). For example, Shen et al. (2012) found that as the angular momentum redistributes, the shell reaches nearly solid-body rotation with a period \sim hundreds of seconds (Figs. 3 and 4 of Shen et al. 2012).

After the merger, carbon is stably burning at the base of the shell, adding degenerate material to the core. At the same time, mass is lost due to the wind. If/when the mass of the core exceeds the Chandrasekhar mass AIC occurs. We associate the prompt short GRB with an AIC *directly* into the neutron star, without formation of an accretion disk. This requirement comes from the observer duration of only ~ 1 second for the short GBRs. If the core is nearly critically rotating before the collapse, with periods of the order of ~ 10 seconds, the accretion time scale is expected to be even longer.

The requirement of a direct collapse demands that the spin of the ONeMg core before the AIC be not too high. To find the conditions for direct collapse consider the rotation of a ONeMg core before the AIC with highly sub-Keplerian velocity on the surface,

$$\Omega_1 R_1 \ll \sqrt{GM_1/R_1} \quad (8)$$

For the direct collapse the final neutron star— should rotate with period $P_{NS} \geq 1$ msec, For a neutron star with radius $R_{NS} = 10$ km the initial period of WD should be

$$P_1 > (R_1/R_{NS})^2 P_{NS} > 90sec. \quad (9)$$

for $R_1/R_{NS} \approx 300$. As we discussed above, Eq. (7), the condition (9) is indeed satisfied following the merger - AIC of the ONeMg core is direct, without formation of the disk. (But the ensuing accretion of the envelope will lead to the formation of the disk, see §6.)

5. Collapse dynamics and magnetic field amplification

Next we consider the dynamics of the inside-out collapse of a polytropic sphere. First we neglect the effects of rotation, assuming a direct radial collapse. Later, we estimate the rotationally-induced shear and the magnetic field amplification within the collapsing star.

5.1. Inside-out collapse of a polytropic sphere

The collapse of a gaseous sphere supported against gravity by the pressure gradients will start from the the center, launching a rarefaction wave propagating to larger radii with the local speed of sound. As a rarefaction wave reaches a given point, the pressure support

against gravity is lost, so that a given fluid element start a nearly free-fall motion in a potential generated by all the material inside this radius. In this Section we discuss the corresponding dynamics for the case of massive WDs.

For analytical estimates, we approximate the WD as a polytropic sphere. Starting with Lane-Emden eq. (Chandrasekhar 1967)

$$\frac{1}{x^2} \partial_x (x^2 \partial_x \theta) = -\theta^n \quad (10)$$

where x is radius, θ is density (in dimensionless unites, whereby $p = \kappa \rho^{1+1/n}$, $\rho = \rho_c \theta^n$, $c_s^2 = \theta c_{s,0}^2$, $c_{s,0}^2 = K \rho_c^{1/n}$ and spatial scales are normalized by

$$r_0 = \sqrt{\frac{n+1}{4\pi G} \kappa \rho_c^{(1-n)/n}} = R_{WD}/x_{max} \quad (11)$$

Time is measured in terms of

$$\tau = \sqrt{\frac{n+1}{4\pi G \rho_c}} = 0.56 \frac{1}{\sqrt{G \rho_c}} \quad (12)$$

For $n = 3$, ($\gamma = 4/3$) the surface is located at $x_{max} = 6.90$ and the total mass is $M_{tot} = 178.3$ (in dimensionless unites). The density θ , relative mass and sound speed as function of x are plotted in Fig. 7. Sound speed is $c_s = c_{s,0} \sqrt{\theta}$. Moment of inertia up to x_0 is

$$J(x_0) = \frac{8\pi}{3} \int_0^{x_0} x^4 \theta(x) dx \quad (13)$$

(rotational energy unto x_0 is $J\Omega_{WD}^2/2$). Total value $J_{tot} = 1867$.

To consider the time-evolution we need to normalize the dimensional factors in the Lane-Emden to a particular WD model. Take $M_{WD} = 1.4M_\odot$ $R_{WD} = 3000$ km. The sound speed at the center is

$$c_{s,0} = \sqrt{\frac{4\pi G \rho_c}{n+1}} r_0 = 1.05 \times 10^8 \frac{\sqrt{\frac{M_{WD}}{M_{Ch}}}}{\sqrt{R_{WD}/3000 \text{ km}}} \text{ cm s}^{-1} \quad (14)$$

Rarefaction wave propagates with sound speed. Integrating $\partial_t r_{RF} = c_s(r_{RF})$, we find the motion of the rarefaction wave, Fig. 8. After the rarefaction wave reaches a point, matter is in a state of near free-fall. Velocity at each point x of the material that started at x_0 is then

$$v = -\sqrt{2M(x_0)(1/x - 1/x_0)}, \quad (15)$$

see Fig. 8.

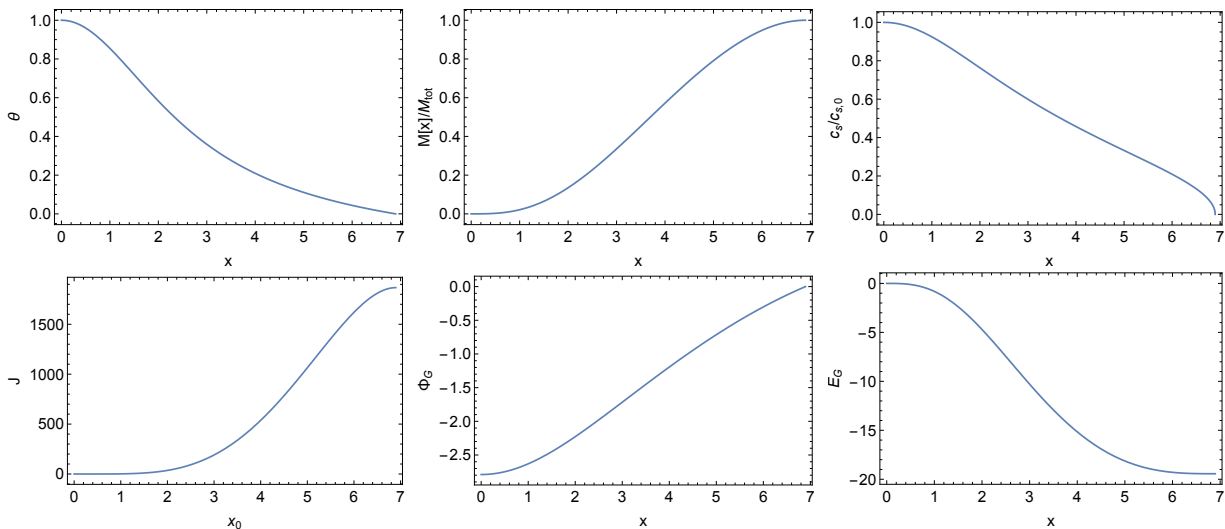


Fig. 7.— Lane-Emden polytropic sphere for $n = 3$. Plotted are: Top row: density (left panel), relative mass (center panel) and sound speed as function of x . Bottom row: Left panel - moment of inertia up to x_0 ; Center panel - gravitational potential as a function of radial coordinate x , Right panel - integrated gravitational energy inside x .

5.2. Accretion shock and the bounce

Let's assume that all the gravitational energy released during collapse is converted into heat and conserved during the evolution (no radiative losses). Knowing the distribution of density $\rho(r)$, parametrized by $\theta(x)$, we can calculate the gravitational potential $\Phi(r)$,

$$\frac{1}{r^2} \partial_r (r^2 \partial_r \Phi) = \rho(r) \quad (16)$$

and gravitational energy up to radius r ,

$$E_g = -\frac{4\pi}{2} \int_0^r \Phi \rho r^2 dr, \quad (17)$$

Fig 7.

Let us next estimate the ram pressure created by the infalling material. Assume that the rarefaction waves reaches radius r at times t . The mass of the shell located between r and $r + c_s dt$ is $dm = 4\pi r^2 \rho(r) c_s dt$. This mass will be accreted during interval

$$\Delta t = \frac{\partial t_{ff}}{\partial r} c_s(r) dt \quad (18)$$

Thus, the ram pressure created by material falling from radius r is

$$p_{ram} = \frac{r^2 v \rho}{r_{in}^2 (\partial t_{ff} / \partial r)} \quad (19)$$

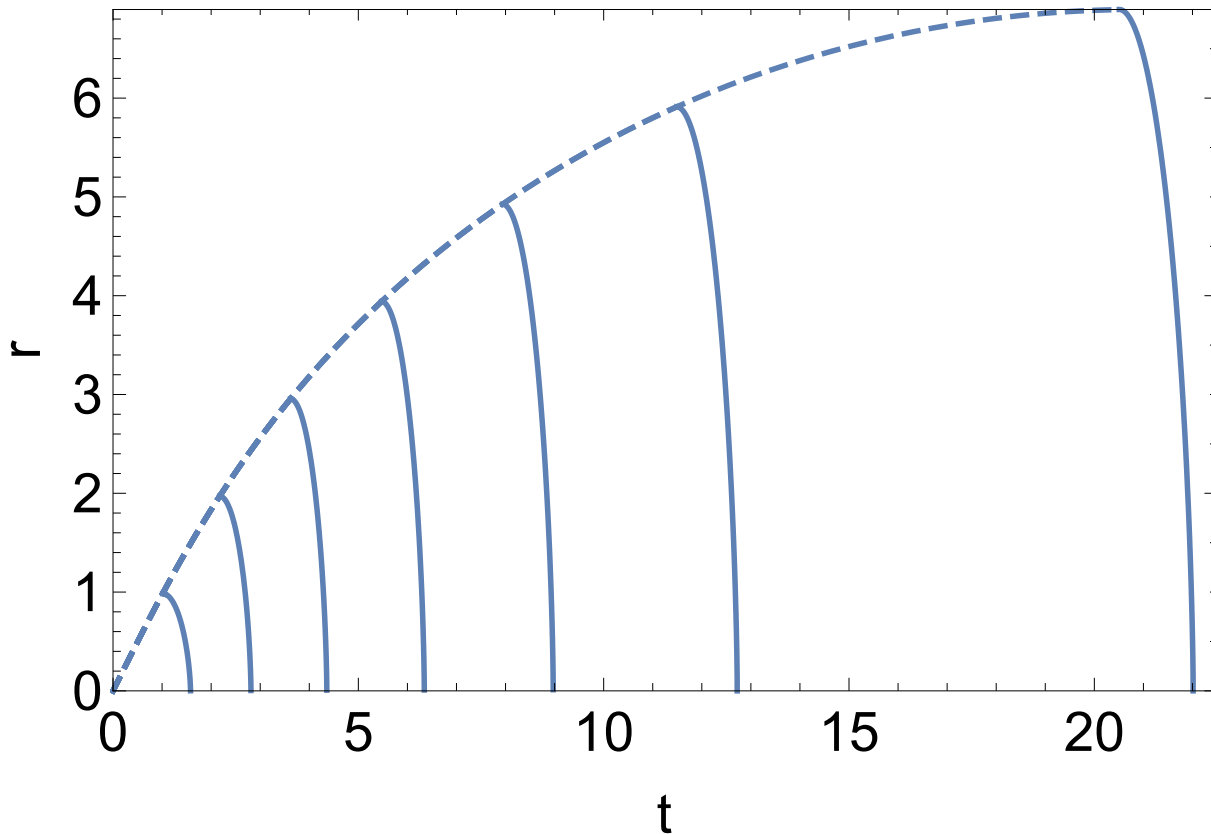


Fig. 8.— Dynamics of the rarefaction wave $r_{RF}(t)$ (dashed line; the surface is reached at $t = 20.89$) and post-rarefaction wave free fall (solid lines are world lines of different elements), dimensionless units, see Eq. (11) and (12).

For $r_{in} \ll r$, $v = \sqrt{2GM_r/r_{in}}$, where, again, M_r is the mass enclosed within the initial radius r . Using (23) we find

$$p_{ram} = \frac{8G}{3\pi} \frac{r^{3/2} M_r^{2/3} \rho}{r_{in}^{5/2} \partial_r (r/M_r^{1/3})} \quad (20)$$

This is the ram pressure created at radius $r_{in} \ll r$ by a material located initially at radius r , Fig. 20.

To estimate the size of the shocked region, we balance the kinetic energy density brought in by the accreting matter, $E_g/(4\pi r_{in}^3/3)$ with ram pressure (9). We find

$$r_{in} = \frac{81}{1024} \frac{E_g \left(\partial_r (r/M_r^{1/3}) \right)^2}{G^2 r^3 M_r^{4/3} \rho^2} \quad (21)$$

This expression locates the accretion shock at time when material from radius r is accreted,

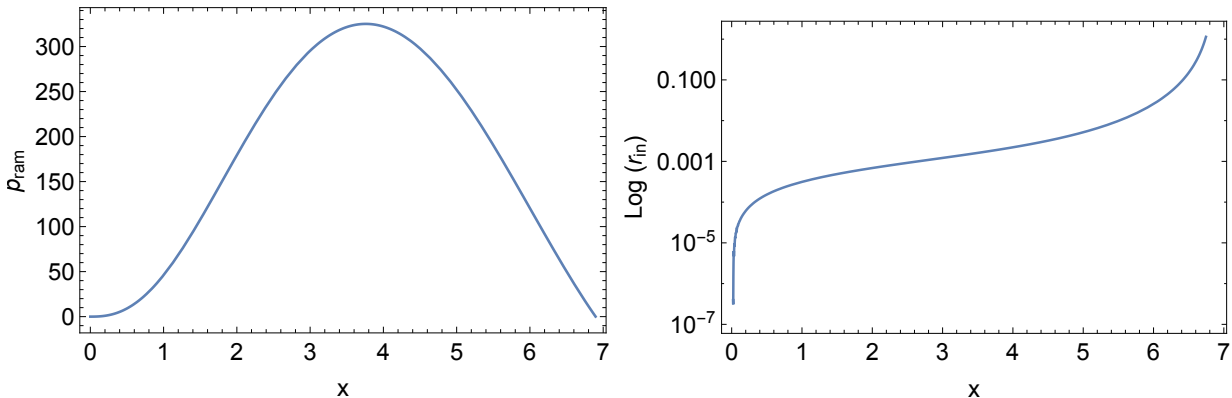


Fig. 9.— Ram pressure created by infalling material initially at dimensionless radius x (left panel) and the location of the accretion shock (right panel). Large values of r_{in} at the end of the collapse correspond to the shock bounce.

Fig. 9.

For most of the accretion time the radius of the shock increases approximately linearly with time. But as the surface approaches the shock the ram pressure decreases dramatically. Since near the surface the density approaches zero linearly (in fact, $\rho \propto 0.044(x_{max} - x)$), we have $r_{in} \propto (x_{max} - x)^{-2}$ - this is the bounce.

5.3. Rotation during collapse

Let’s consider rotational evolution during collapse. As a fiducial estimate, let’s assume that WD of $R_{WD} = 3000$ km collapses to $R_{NS} = 30$ km, by a factor 1/100, to $x_{min} = x_{max}/100$. (Further contraction is expected during cooling.)

We employ the following model of the collapse: (i) we separate the star into weakly rotating outer parts, unaffected by the rarefaction wave, (ii) a free-fall region, (ii) a core. We assume that the core has a radius much smaller than the initial configuration, so that at each moment its mass and angular speed are determined by the amount of the material and angular momentum that has reached the point $r = 0$ before a given moment. We assume that the radial infall dynamics is unaffected by the rotation (hence the requirement of sufficiently slow rotation discussed above.)

Let’s assume that the central object has the same gyro-ratio as the initial WD: $\eta_0 = 0.22$. Then, after material from x_0 accreted on the central object, conservation of angular

momentum gives

$$J(x_0)\Omega_{WD} = \eta_0 x_{min}^2 M(x_0)\omega_c \quad (22)$$

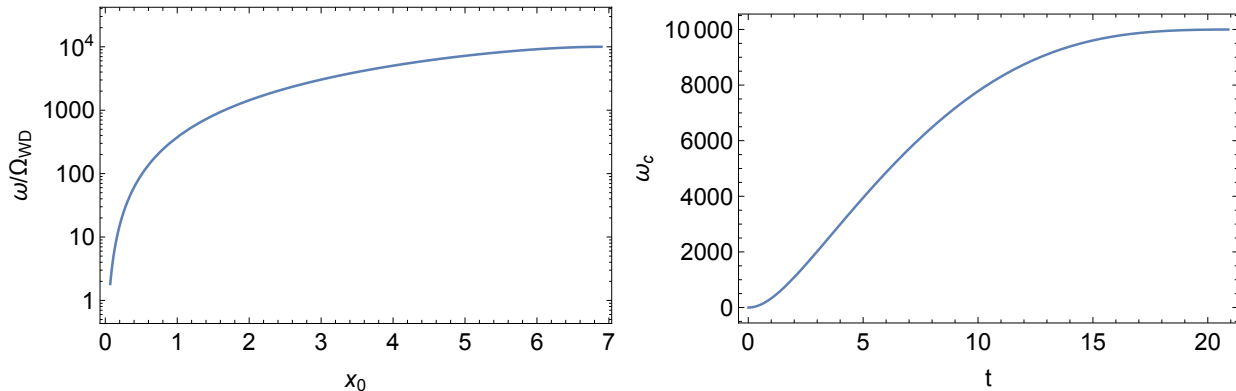


Fig. 10.— Left Panel: Angular velocity of the central object as function of the initial position of the accreted shells. Right panel: angular velocity of the central object as function of time. Maximal value is $\omega/\Omega_{WD} = (x_{max}/x_{min})^2 = 10^4$.

Let us then calculate the temporal evolution of the angular velocity of the central object. It may be demonstrated that (in physical units) the free-fall time t_{ff} from a location r that encloses mass M_r is

$$t_{ff} = \frac{\pi}{2\sqrt{2}} \frac{r^{3/2}}{\sqrt{GM_r}} \quad (23)$$

Interestingly, for a polytropic EoS this gives a final time even for $r = 0$ (since $M_r \propto r^3$ for small r , $t_{ff} = 0.96\tau$). To account for this mathematical oddity, we subtract from (23) a value for $r = 0$. In terms of the dimensionless time,

$$t_{ff} \equiv \frac{t_{ff}}{\tau} = 1.968 \frac{x_0^{3/2}}{M(x_0)} - 0.96, \quad (24)$$

For the surface layer $t_{ff}(x_{max}) = 1.70$. The angular velocity of the core is then, Fig. 10,

$$\omega_c(t) = \frac{J(t)}{\eta_0 x_{min}^2 M(t)}. \quad (25)$$

5.4. Magnetic field amplification

Previously magnetic field amplification during collapse was considered by Thompson & Duncan (1995). They argued that *if* the accretion is direct, without the formation of the

accretion disk, magnetic field can be amplified by an $\alpha - \omega$ dynamo, while the star can be spun to millisecond periods. A simple flux conservation gives $B_{NS} \approx (R_{WD}/R_{NS})^2 B_{WD} \approx 10^{12} \text{G} B_{WD,8}$. Thompson & Duncan (1995) argued that twisting of the magnetic field during collapse and ensuing dynamo action can bring the magnetic field to magnetar values. In what follows we use the above-given calculations of the infall, add rotation, and estimate the resulting magnetic field. We find that even without dynamo action the magnetic field can be twisted to magnetar values.

As the star collapses, differential rotation will lead to amplification of the toroidal magnetic field. To estimate the magnetic field amplification, we assume that the initial configuration is mostly poloidal. Then the resulting toroidal field will be larger than the final poloidal field approximately by the difference in the number of turns between the core and the outer layer. To estimate the the number of turns that the core makes, we integrate $\omega_c(t)$, Eq. (25) over collapse time,

$$N_c = \frac{1}{2\pi} \int \omega_c(t) dt = 2.2 \times 10^4 \quad (26)$$

Before the RF reached the outer layer, it rotates with the initial Ω_{WD} ; in addition, as the outer layer falls onto the star it's rotational velocity increases. We find for the number of turns of the outer layer

$$N_{outer} = 6.7 \quad (27)$$

The fact that the total winding of the toroidal magnetic field, Eq. (26), reaches $\sim 10^4$ has a simple order-of-magnitude explanation: the collapse takes about 2 dynamical times from the center to the surface (for RF and the ensuing free-fall). Typically the core rotates with $\omega_c \sim (x_{out}/x_{in})^2 \Omega$, while the outer layer rotates with Ω . For $x_{out}/x_{in} \sim 100$ this gives $\omega_c \sim 10^4$.

Thus, the toroidal magnetic field can be $\sim 10^4$ times higher than the poloidal. In addition, poloidal magnetic field will be amplified by flux conservation. For example, if we start with $B_{WD} \sim 10^6$ G, flux conservation will give a factor $(x_{max}/x_{min})^2 \approx 10^4$, while differential rotation will further boost that by $\sim 2.2 \times 10^4$, reaching magnetar-like values of $B \geq B_Q$.

6. The extended emission (EE) and the final NS

6.1. Shell forms a Keplerian disk around newly formed NS

As our basic scenario of the post-merger evolution we chose the left column of Fig. 2 - no prompt collapse, CO shell burning and AIC after the core exceeds M_{Ch} . For definiteness let's assume that the mass of the shell at the moment of AIC is $M_d \sim 0.5M_\odot$, its typical radius is $R_s \sim 5 \times 10^9$ cm (see *e.g.* Shen et al. 2012), and it is rotating with the period $P_s \sim 10^3$ sec. The neutron star has its magnetic field amplified to nearly critical values and is spinning at few milliseconds.

The material of the shell has a proper angular momentum $\sim \Omega_s R_s^2$. After the loss of support from the core, the shell will form a disk at the radius R_K where this proper angular momentum corresponds to Keplerian rotation,

$$\begin{aligned} \Omega_s R_s^2 &= \sqrt{GM_{NS} R_K} \rightarrow \\ R_K &= \frac{R_s^4 \Omega_s^2}{GM_{NS}} = 10^8 \left(\frac{R_s}{5 \times 10^9 \text{ cm}} \right)^4 \left(\frac{P_s}{10^3 \text{ sec}} \right)^{-2} \text{ cm} \\ \Omega_K &= \frac{(GM_{NS})^2}{R_s^6 \Omega_s^3} = 10 \left(\frac{R_s}{5 \times 10^9 \text{ cm}} \right)^{-6} \left(\frac{P_s}{10^3 \text{ sec}} \right)^{-3} \text{ rad s}^{-1} \end{aligned} \quad (28)$$

Thus, the newly formed disk rotates with a period P_K of the order of a second.

It is expected that the accretion time, *e.g.* within the α -prescription,

$$\tau_{acc} \sim \frac{P_K}{\alpha} \left(\frac{R_d}{H_d} \right)^2 \quad (29)$$

will be $\sim 1/\alpha \approx 10 - 100$ times longer than the period (assuming that $R_d \sim H_d$ and $\alpha = 10^{-2} - 10^{-1}$). Thus the accretion rate will be of the order

$$\dot{M} \approx \alpha \frac{\Delta M}{P_K} \approx 10^{-3} M_\odot \text{s}^{-1} \quad (30)$$

Typical accretion time scale

$$\tau \sim \frac{M_d}{\dot{M}} \approx \frac{P_K}{\alpha} \approx 100 \text{ sec} \quad (31)$$

This is the extended emission (EE).

Accretion of material onto the NS is a famously complicated problem. As basic estimate we note, that the accretion rate (30) is so high, that the Alfvén radius could be smaller than the NS radius

$$\frac{r_A}{r_{NS}} = \frac{2^{4/7} \pi^{2/7} B_{NS}^{4/7} R_{NS}^{5/7}}{GM^{1/7} \dot{M}^{2/7}} = 0.9 \left(\frac{B_{NS}}{B_Q} \right)^{4/7} \quad (32)$$

Thus, direct accretion on the NS can occur even for magnetar-like fields (B_Q is critical quantum field magnetic field).

For somewhat different sets of parameters, the shell will be ejected in a propeller regime (Lipunov et al. 1992; Ustyugova et al. 2006), when the magnetospheric radius is larger than the corotation radius and smaller than the light cylinder radius. In this case most of the matter is expelled radially in the equatorial plane by the rotating magnetosphere of the star.

The expected upper limit on the EE luminosity, accretion-powered, can be estimated as

$$L_{EE} \approx \eta_a \dot{M} c^2 \frac{R_{NS}}{R_G} = 7 \times 10^{49} \eta_{-1} \text{ ergs}^{-1} \quad (33)$$

where $\eta_{a,-1} = \eta_a/10^{-1}$ is the efficiency of converting accretion power into radiation. This is comparable to the observer EE power.

We also point out that accretion in this case happens in an interesting, not yet explored regime: very high \dot{M} on to rapidly spinning ultra-magnetized neutron star. In certain regimes accretion will proceed in the propeller regime, so that a large amount of rotational energy of the neutron star is given to the ejected material (Piro & Ott 2011).

6.2. Afterglows: pulsar-like termination shock in fast wind

As a result of the AIC a highly spinning, with a period few milliseconds, NS is born. At the same time magnetic field can be amplified to magnetar fields. Importantly, after all the secondary material is accreted the nature of the collimation changes: isolate neutron stars lose most of it's rotational energy *in the equatorial plane*, with luminosity $L \propto \sin^2 \theta$, where θ is the polar angle. The highly magnetized relativistic wind produced by a central neutron star will interact with the fairly dense newly ejected material and dense pre-AIC wind, producing *X-ray afterglow in the highly magnetized reverse shock*, in a way similar to the case of afterglows from long GRBs (Lyutikov & Camilo Jaramillo 2017).

7. Discussion

We advance a model of short GRBs originating from unstable mass transfer (merger of) from a CO WD onto a heavy ONeMg WD. The disrupted CO WD enters a shell burning stage, adds material to the core of primary, which experiences the accretion induced collapse. During AIC the magnetic field is amplified, while the remaining shell provides a collimation of the outflow. Accretion continues onto the newly formed NS from the disrupted companion,

producing extended emission. At later stages pulsar winds interact with the pre-collapse wind (and possibly with the shell ejected in a propeller regime of accretion) and produces afterglows by particle acceleration at the termination shock, similar to Pulsar Wind Nebulae and what has been suggested by long GRBs (Lyutikov & Camilo Jaramillo 2017).

The model explains both the prompt GRB stage - around the bounce time - and the extended emission - due to shell accretion. Additional flaring activity may be produced by the newly born neutron star via magnetar-like flares. In addition mild optical signal is expected during the AIC of the WD (*e.g.* material ejected during the bounce interacting with the remaining accretion disk). We do not expect in this case the GRBs to be associated with a strong gravitational wave signal.

Qualitatively, the model allows for a larger variety of properties of short GRBs than the standard NS-NS merge paradigm. The most important macroscopic variable parameters are the masses of the WDs before the merger (this depends on the initial masses and separation), and pre-AIC rotational periods of the shell and the core. In addition, there is a possibility that AIC occurs during the active stage of the CO WD disruption.

Importantly, it is *required* that the proposed scenario be very rare, accounting to at most only few percent of the WD mergers (or at most 10% of super-Chandrasekhar mergers). Other (majority of) channels may lead either to SN Ia explosions or very weak transients. Only the right combination(s) of initial masses and separations should lead to short GRBs associated with WD mergers.

The present model postulates a fairly dense surrounding of short GRBs (due to the presence of unburnt shell and the powerful pre-AIC wind) in contrast to a very clean circumburst environment of NS-NS mergers. We view it as a strong point of the model - both long and short GRBs have tenths to few solar masses of the material in the immediate surrounding of the explosion (smaller for shorter bursts). This leads to similarly looking early afterglows, just somewhat less energetic in case of short GRBs. The model also qualitatively explains these long-short GRBs similarities as both being powered by an ultra-relativistic highly magnetized wind, produce, *e.g.* by a millisecond highly magnetized neutron star in both cases.

The present model offers a number of possibly interesting developments:

- Interaction of the AIC bounce ejecta with the envelope. We expect that $M_{ej} \sim 10^{-3} - 10^{-2} M_{\odot}$ are ejected during AIC with mildly relativistic velocities, *e.g.* with $v_{ej} \sim c/3$, the sound speed in relativistic fluid. The total energy of the ejecta can be $\sim 10^{50} - 10^{51}$ ergs. This ejecta immediately runs into $M_s \sim \text{few} \times 10^{-1} M_{\odot}$ shell. By conservation of

the momentum, the resulting shell will be moving with velocity

$$v_s \sim \frac{c M_{ej}}{3 M_s} \sim 10^9 \text{ cm s}^{-1} \quad (34)$$

The shell will be heated to

$$T \sim \frac{m_p c^2 M_{ej}}{18 M_s} \sim \text{few MeV} \quad (35)$$

Thus, the interaction of the AIC bounce ejecta with the shell will produce a very dirty GRB, with long time scales and lower photon energies.

- Shock breakout from the shell. The AIC bounce ejecta will launch a shock in the shell. During the breakout of the shock, the top material will be accelerated to mildly relativistic velocities, even though the bulk of the shell material moves non-relativistically, Eq (34)
- Interaction of the shell with the pre-AIC wind produces directionally anisotropic radiation features, Fig. 11. For example, shell ejection is a propeller regime and pulsar-generated wind will be equatorially collimated, yet in “strong propeller” regime (Ustyugova et al. 2006) collimated magnetically dominated outflow can be present as well.

We would like to thank Chris Fryer, Natasha Ivanona, Mansi Kasliwal, Marten van Kerkwijk, Patrick Motl, Kelly Lepo, Lorne Nelson, Thomas Tauris, Sterl Phinney, Tony Piro, Philipp Podsiadlowski, Jan Staff, Ken Shen, and organizers of NORDITA workshop The Physics of Extreme-Gravity Stars, and Samaya Nissanke in particular. This work was supported by NSF grant AST-1306672 and DoE grant DE-SC0016369.

REFERENCES

- Abdikamalov, E. B., Ott, C. D., Rezzolla, L., Dessart, L., Dimmelmeier, H., Marek, A., & Janka, H.-T. 2010, *Phys. Rev. D*, 81, 044012
- Baiotti, L. & Rezzolla, L. 2017, *Reports on Progress in Physics*, 80, 096901
- Balsara, D. S., Fisker, J. L., Godon, P., & Sion, E. M. 2009, *ApJ*, 702, 1536
- Belyaev, M. A., Rafikov, R. R., & Stone, J. M. 2013, *ApJ*, 770, 67
- Benz, W., Bowers, R. L., Cameron, A. G. W., & Press, W. H. . 1990, *ApJ*, 348, 647
- Berger, E. 2010, *ApJ*, 722, 1946

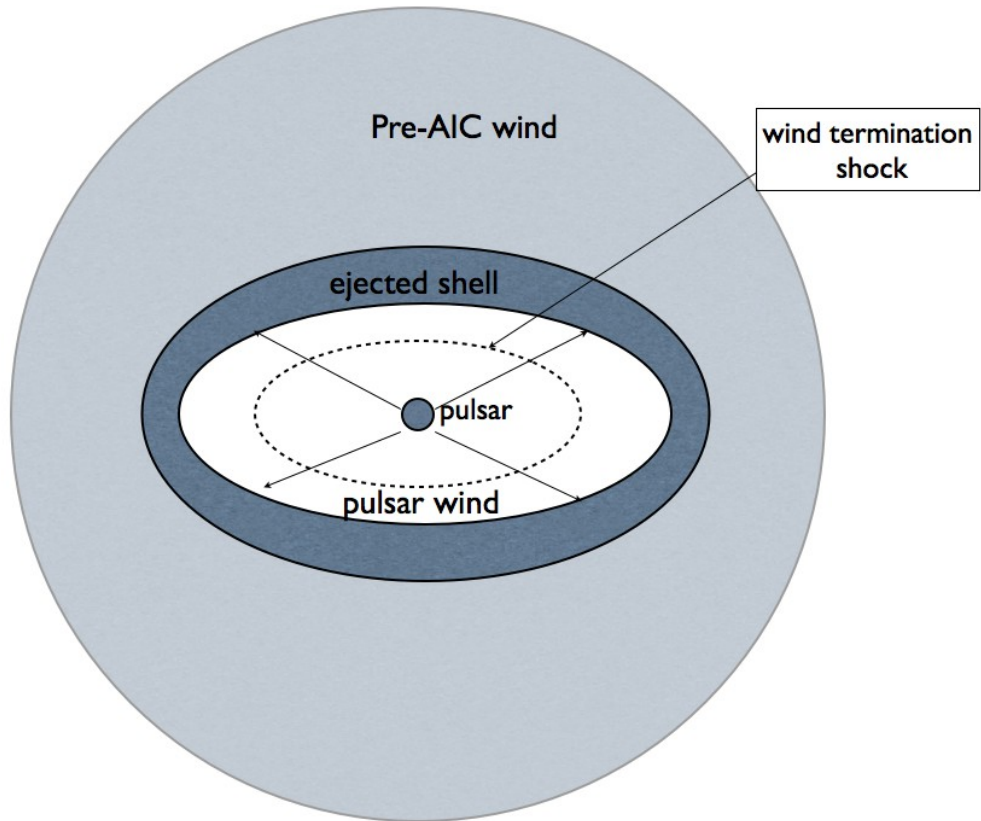


Fig. 11.— Immediate surrounding of a short GRB: the remaining NS generates pulsar-like wind (highly relativistic, highly magnetized), that interacts with the shell ejected in a propeller regime, and the wind from the shell burning stage. Both pulsar winds and the ejected shell are equatorially collimated. Early afterglows are produced at the wind termination shock, similar to the case of long GRBs discussed by Lyutikov & Camilo Jaramillo (2017)

—. 2014, *ARA&A*, 52, 43

Bhattacharya, D. & van den Heuvel, E. P. J. 1991, *Phys. Rep.*, 203, 1

Bobrick, A., Davies, M. B., & Church, R. P. 2017, *MNRAS*, 467, 3556

Bucciantini, N., Quataert, E., Arons, J., Metzger, B. D., & Thompson, T. A. 2008, *MNRAS*, 383, L25

Burrows, A., Dessart, L., Livne, E., Ott, C. D., & Murphy, J. 2007, *ApJ*, 664, 416

- Canal, R. & Schatzman, E. 1976, *A&A*, 46, 229
- Cappellaro, E. & Turatto, M. 2001, in *ASSL*, Vol. 264, *The Influence of Binaries on Stellar Population Studies*, ed. D. Vanbeveren (Dordrecht: Kluwer Academic Publishers), 199
- Chandrasekhar, S. 1967, *An introduction to the study of stellar structure*
- Claeys, J. S. W., Pols, O. R., Izzard, R. G., Vink, J., & Verbunt, F. W. M. 2014, *A&A*, 563, A83
- Coward, D. M., Howell, E. J., Piran, T., Stratta, G., Branchesi, M., Bromberg, O., Gendre, B., Burman, R. R., & Guetta, D. 2012, *MNRAS*, 425, 2668
- Dan, M., Rosswog, S., Brügggen, M., & Podsiadlowski, P. 2014, *MNRAS*, 438, 14
- Dessart, L., Burrows, A., Livne, E., & Ott, C. D. 2007, *ApJ*, 669, 585
- Dessart, L., Burrows, A., Ott, C. D., Livne, E., Yoon, S.-C., & Langer, N. 2006, *ApJ*, 644, 1063
- Dessart, L., Ott, C. D., Burrows, A., Rosswog, S., & Livne, E. 2009, *ApJ*, 690, 1681
- D’Souza, M. C. R., Motl, P. M., Tohline, J. E., & Frank, J. 2006, *ApJ*, 643, 381
- Duncan, R. C. & Thompson, C. 1992, *ApJ*, 392, L9
- Eggleton, P. P. 1983, *ApJ*, 268, 368
- Faber, J. A. & Rasio, F. A. 2012, *Living Reviews in Relativity*, 15, 8
- Fryer, C., Benz, W., Herant, M., & Colgate, S. A. 1999, *ApJ*, 516, 892
- Gehrels, N., Ramirez-Ruiz, E., & Fox, D. B. 2009, *ArXiv e-prints*
- Hotokezaka, K., Kyutoku, K., Okawa, H., Shibata, M., & Kiuchi, K. 2011, *Phys. Rev. D*, 83, 124008
- Hurley, J. R., Tout, C. A., Wickramasinghe, D. T., Ferrario, L., & Kiel, P. D. 2010, *MNRAS*, 402, 1437
- Iben, Jr., I. 1988, *ApJ*, 324, 355
- Iben, Jr., I. & Livio, M. 1993, *PASP*, 105, 1373

- Inogamov, N. A. & Sunyaev, R. A. 1999, *Astronomy Letters*, 25, 269
- . 2010, *Astronomy Letters*, 36, 848
- Ivanova, N., Justham, S., Chen, X., De Marco, O., Fryer, C. L., Gaburov, E., Ge, H., Glebbeek, E., Han, Z., Li, X.-D., Lu, G., Marsh, T., Podsiadlowski, P., Potter, A., Soker, N., Taam, R., Tauris, T. M., van den Heuvel, E. P. J., & Webbink, R. F. 2013, *A&A Rev.*, 21, 59
- Kawai, Y., Saio, H., & Nomoto, K. 1987, *ApJ*, 315, 229
- King, A. R., Pringle, J. E., & Wickramasinghe, D. T. 2001, *MNRAS*, 320, L45
- Kitaura, F. S., Janka, H.-T., & Hillebrandt, W. 2006, *A&A*, 450, 345
- Komissarov, S. S. & Lyubarsky, Y. E. 2003, *MNRAS*, 344, L93
- . 2004, *MNRAS*, 349, 779
- Komissarov, S. S., Vlahakis, N., Königl, A., & Barkov, M. V. 2009, *MNRAS*, 394, 1182
- Langer, N. 2012, *ARA&A*, 50, 107
- Lee, W. H. & Ramirez-Ruiz, E. 2007, *New Journal of Physics*, 9, 17
- Levan, A. J., Wynn, G. A., Chapman, R., Davies, M. B., King, A. R., Priddey, R. S., & Tanvir, N. R. 2006, *MNRAS*, 368, L1
- Lipunov, V. M., Börner, G., & Wadhwa, R. S. 1992, *Astrophysics of Neutron Stars*, 108
- Lyutikov, M. 2009, *ArXiv e-prints* 0911.0349
- Lyutikov, M. & Camilo Jaramillo, J. 2017, *ApJ*, 835, 206
- MacFadyen, A. I. & Woosley, S. E. 1999, *ApJ*, 524, 262
- Maoz, D. & Graur, O. 2017, *ArXiv e-prints*
- Maoz, D., Mannucci, F., & Nelemans, G. 2014, *ARA&A*, 52, 107
- Marsh, T. R., Nelemans, G., & Steeghs, D. 2004, *MNRAS*, 350, 113
- Mennekens, N., Vanbeveren, D., De Greve, J. P., & De Donder, E. 2010, *A&A*, 515, A89
- Metzger, B. D., Giannios, D., Thompson, T. A., Bucciantini, N., & Quataert, E. 2011, *MNRAS*, 413, 2031

- Metzger, B. D., Piro, A. L., & Quataert, E. 2009a, MNRAS, 396, 1659
- Metzger, B. D., Piro, A. L., Quataert, E., & Thompson, T. A. 2009b, ArXiv e-prints
- Metzger, B. D., Quataert, E., & Thompson, T. A. 2008, MNRAS, 385, 1455
- Michel, F. C. 1973, ApJ, 180, L133
- Miyaji, S., Nomoto, K., Yokoi, K., & Sugimoto, D. 1980, PASJ, 32, 303
- Mochkovitch, R. & Livio, M. 1990, A&A, 236, 378
- Motl, P. M., Frank, J., Staff, J., Clayton, G. C., Fryer, C. L., Even, W., Diehl, S., & Tohline, J. E. 2017, ApJS, 229, 27
- Motl, P. M., Frank, J., Tohline, J. E., & D’Souza, M. C. R. 2007, ApJ, 670, 1314
- Nakar, E. & Sari, R. 2012, ApJ, 747, 88
- Nelemans, G., Verbunt, F., Yungelson, L. R., & Portegies Zwart, S. F. 2000, A&A, 360, 1011
- Nomoto, K. & Iben, Jr., I. 1985, ApJ, 297, 531
- Norris, J. P. & Bonnell, J. T. 2006, ApJ, 643, 266
- Norris, J. P., Gehrels, N., & Scargle, J. D. 2010, ApJ, 717, 411
- Paczynski, B. 1971, ARA&A, 9, 183
- Pakmor, R., Kromer, M., Röpke, F. K., Sim, S. A., Ruiter, A. J., & Hillebrandt, W. 2010, Nature, 463, 61
- Pakmor, R., Kromer, M., Taubenberger, S., & Springel, V. 2013, ApJ, 770, L8
- Paschalidis, V. 2017, Classical and Quantum Gravity, 34, 084002
- Paschalidis, V., Ruiz, M., & Shapiro, S. L. 2015, ApJ, 806, L14
- Paschalidis, V. & Stergioulas, N. 2016, ArXiv e-prints
- Philippov, A. A., Rafikov, R. R., & Stone, J. M. 2016, ApJ, 817, 62
- Piro, A. L. & Kulkarni, S. R. 2013, ApJ, 762, L17
- Piro, A. L. & Ott, C. D. 2011, ApJ, 736, 108

- Podsiadlowski, P., Langer, N., Poelarends, A. J. T., Rappaport, S., Heger, A., & Pfahl, E. 2004, *ApJ*, 612, 1044
- Portegies Zwart, S. F. & Verbunt, F. 1996, *A&A*, 309, 179
- Raskin, C., Scannapieco, E., Fryer, C., Rockefeller, G., & Timmes, F. X. 2012, *ApJ*, 746, 62
- Rezzolla, L., Baiotti, L., Giacomazzo, B., Link, D., & Font, J. A. 2010, *Classical and Quantum Gravity*, 27, 114105
- Rezzolla, L., Giacomazzo, B., Baiotti, L., Granot, J., Kouveliotou, C., & Aloy, M. A. 2011, *ApJ*, 732, L6
- Ruiz, M., Lang, R. N., Paschalidis, V., & Shapiro, S. L. 2016, *ApJ*, 824, L6
- Saio, H. & Nomoto, K. 1985, *A&A*, 150, L21
- Schwab, J., Quataert, E., & Bildsten, L. 2015, *MNRAS*, 453, 1910
- . 2016, *MNRAS*, 458, 3613
- Sekiguchi, Y., Kiuchi, K., Kyutoku, K., & Shibata, M. 2011, *Physical Review Letters*, 107, 051102
- Shen, K. J. 2015, *ApJ*, 805, L6
- Shen, K. J., Bildsten, L., Kasen, D., & Quataert, E. 2012, *ApJ*, 748, 35
- Shen, K. J., Kasen, D., Miles, B. J., & Townsley, D. M. 2017, *ArXiv e-prints*
- Shibata, M., Kiuchi, K., & Sekiguchi, Y.-i. 2017, *Phys. Rev. D*, 95, 083005
- Siess, L. 2006, *A&A*, 448, 717
- Staff, J. E., Menon, A., Herwig, F., Even, W., Fryer, C. L., Motl, P. M., Geballe, T., Pignatari, M., Clayton, G. C., & Tohline, J. E. 2012, *ApJ*, 757, 76
- Tauris, T. M., Langer, N., & Kramer, M. 2012, *MNRAS*, 425, 1601
- Tauris, T. M., Sanyal, D., Yoon, S.-C., & Langer, N. 2013, *A&A*, 558, A39
- Thompson, C. & Duncan, R. C. 1995, in *Astronomical Society of the Pacific Conference Series*, Vol. 72, *Millisecond Pulsars. A Decade of Surprise*, ed. A. S. Fruchter, M. Tavani, & D. C. Backer, 301

- Toonen, S., Claeys, J. S. W., Mennekens, N., & Ruiter, A. J. 2014, *A&A*, 562, A14
- Toonen, S., Hollands, M., Gänsicke, B. T., & Boekholt, T. 2017, *A&A*, 602, A16
- Toonen, S. & Nelemans, G. 2013, *A&A*, 557, A87
- Toonen, S., Nelemans, G., & Portegies Zwart, S. 2012, *A&A*, 546, A70
- Townsley, D. M. & Bildsten, L. 2005, *ApJ*, 628, 395
- Usov, V. V. 1992, *Nature*, 357, 472
- Ustyugova, G. V., Koldoba, A. V., Romanova, M. M., & Lovelace, R. V. E. 2006, *ApJ*, 646, 304
- van Kerkwijk, M. H., Chang, P., & Justham, S. 2010, *ApJ*, 722, L157
- Vietri, M. & Stella, L. 1999, *ApJ*, 527, L43
- Voss, R. & Tauris, T. M. 2003, *MNRAS*, 342, 1169
- Wang, B. & Han, Z. 2012, *New A Rev.*, 56, 122
- Webbink, R. F. 1984, *ApJ*, 277, 355
- Webbink, R. F. & Iben, Jr., I. 1987, in *IAU Colloq. 95: Second Conference on Faint Blue Stars*, ed. A. G. D. Philip, D. S. Hayes, & J. W. Liebert, 445–456
- Woosley, S. E. & Baron, E. 1992, *ApJ*, 391, 228
- Yoon, S.-C., Podsiadlowski, P., & Rosswog, S. 2007, *MNRAS*, 380, 933